ORIGINAL RESEARCH ARTICLE

A Multifunctional Lead-Free Ferroelectric Transparent Ceramic $(K_{0.5}Na_{0.5})NbO_3$ Modified by $Sr(Bi_{0.5}Nb_{0.5})O_3$ with High Transmittance

Chengjian Yu[1] · Haonan Liu[1] · Liwen Wang[1] · Kaishuo Liu[1] · Hua Wang[1,2] · Jiwen Xu[1,2] · Ling Yang[1] · Wei Qiu[1]

Abstract

$(1-x)(K_{0.5}Na_{0.5})NbO_3$-$xSr(Bi_{0.5}Nb_{0.5})O_3$ (KNN-xSBN, $x = 0.02, 0.03, 0.04, 0.05, 0.06, 0.07$) ceramics were designed and prepared by solid-phase method. The effects of different SBN content in solid solution on the transmittance, microstructure, phase structure, ferroelectric properties, and energy storage properties of ceramic samples were studied. After adding the second component SBN, the phase structure of KNN ceramics changes from tetragonal phase structure to cubic phase structure, and the grain size reaches the micron level, so that it exhibits good light transmittance and also retains good ferroelectricity, energy storage, and other performance parameters. It is a multifunctional material with excellent performance. When $x = 0.06$, the transmittance of the ceramic sample is the highest; the transmittance in the visible light band (780 nm) reaches 64.64%, and the transmittance in the near-infrared band reaches 71.68% (1100 nm); when $x = 0.07$, energy storage efficiency η reaches 74%.

Keywords Transparent ceramics · lead-free · ferroelectric ceramics · energy storage

Introduction

With the rapid development of the optoelectronics industry, research and preparation of new multifunctional materials has increasingly become a hot research direction. Polycrystalline transparent ceramics have gradually become a key research direction due to their excellent versatility and are widely used in optoelectronics due to their high hardness, high thermal stability, and optoelectronic properties.[1–4] At present, lead-based ceramics occupy an important position in the field of optoelectronics. However, with the increasingly serious environmental problems and the enhanced environmental awareness, alternative materials are being sought to replace lead-containing ceramics that cause great damage to the human body and the environment.[5–8] Therefore, it is essential to find new lead-free ceramics to replace lead-based ceramics. KNN-based ceramics have been widely used in various fields due to their high dielectric constant, piezoelectric constant, and high electromechanical coupling coefficient at room temperature, as well as good optical transmittance. A number of smarter methods of KNN synthesis were developed, for example, via sol–gel,[9–11] hydrothermal,[12] or solution routes.[13] They are, however, less suitable for industrial production than a solid-state route. The solid-phase synthesis method is widely used because the ceramics produced by this method have excellent chemical stability and good thermal stability, which ensures that they maintain a stable structure and properties at high temperatures and are not easily deformed or destroyed, making them suitable for high-temperature applications. KNN is also widely used due to its excellent dielectric properties. Kannan et al. used the solid-state reaction method to fabricate KNN-CS ceramics with high dielectric and piezoelectric properties. KNN-CS ceramics are employed as substitutes for lead (Pb)-based materials in sensor applications.[14] Gao et al. utilized dielectric properties of KNN in the frequency range of 8.2–12.4 GHz to develop KNN/Al$_2$O$_3$ microwave-absorbing ceramic.[15] Wang et al. analyzed the conductive and dielectric relaxation mechanisms, and provided an approach for future industrial applications where p-type conductivity could be achieved by doping KNN ceramics.[16] KNN-based ceramic materials will be an ideal alternative to lead-based materials.[17–20]

✉ Hua Wang
wh65@tom.com

1 School of Materials Science and Engineering, Guilin University of Electronic Technology, Guilin 541004, People's Republic of China

2 Guangxi Key Laboratory of Information Materials, Guilin University of Electronic Technology, Guilin 541004, People's Republic of China

Among transparent ferroelectric ceramics, KNN-based lead-free ceramics have received extensive attention.[20–24] Kwork et al. reported KNN-based ceramics with relatively high transmittance of 60% in the visible and near-infrared (IR) regions and high electro-optic coefficients.[25] Du et al. also reported that $(K_{0.5}Na_{0.5})NbO_3$-$Sr(Sc_{0.5}Nb_{0.5})O_3$-based ceramics have a transmittance of up to 60% in the visible region and a moderate energy storage density.[26] A large number of experimental results have verified that the transparent fluorescent ferroelectric ceramics prepared by doping a second component into KNN-based transparent ceramics have the characteristics of high transmittance and good stability, providing an excellent multifunctional material. For instance, the grain size of KNN-based ceramics changes from 3 to 4 μm to 0.6 μm after doping with $Bi_{0.5}(Na_{0.925}Li_{0.075})_{0.5}ZrO_3$, and the transparency is obviously improved.[27] Geng et al. reported that $[(K_{0.5}Na_{0.5})_{1-2x}(Sr_{0.75}Ba_{0.25})_x]_{0.93}Li_{0.07}Nb_{0.93}Bi_{0.07}O_3$ ceramics have uniform and fine grain size, as well as a high transmittance of 60% in the near-IR region.[28]

Previous studies have shown that doping the second component can effectively manipulate the phase structure and reduce the grain size, which plays a key role in the transmittance of KNN-based ceramics. Wu et al. studied the improvement of phase structure and light performance of KNN by BBT.[29] The results show that BBT led to a certain improvement in the transmittance and energy storage of KNN. However, because the grain size is not small enough, there is still room for improvement in light transmittance. So we wanted to find other second elements to make the grain size even smaller and achieve better optoelectronic performance. In this paper, KNN ceramics with good electrical properties were selected as the substrate to explore the effect of solid solution SBN on the phase structure, grain size, and microstructure of KNN ceramic samples. By introducing SBN, Sr^{2+} replaces some K^+ and Na^+, and Nb^{5+} and Bi^{3+} occupy the B position. In this way, the phase structure can be effectively regulated, and the grain size is reduced to achieve uniform grain distribution. As a result, the transmittance, ferroelectric, and energy storage properties of the ceramic samples are improved.[30,31] At the same time, it is also necessary to explore the optimal solid solution content of the second component and the reasonable firing system of the ceramic samples, and finally, find the formula composition with the highest light transmission performance and the solid solution content of the second component.

Experimental Details

$(1-x)(K_{0.5}Na_{0.5})NbO_3$-$xSr(Bi_{0.5}Nb_{0.5})O_3$ ($x = 0.02$, 0.03, 0.04, 0.05, 0.06, 0.07) ceramics were prepared by solid-phase preparation. The raw materials are K_2CO_3 (99.9%), Na_2CO_3 (99.9%), Nb_2O_5 (99.99%), $SrCO_3$ (99.99%), and Bi_2O_3 (99.999%), weighed according to the stoichiometric ratio. The raw materials were put it into a nylon grinding jar with ZrO as the grinding ball and mixed with anhydrous ethanol for 24 h. After the ball-milled powder was dried, it was calcined at 860°C for 2 h. The calcined powder was poured into a ball mill tank for the second ball milling with the same conditions as primary ball milling. The powder after the secondary ball milling was dried and then calcined again. The sintering conditions of the secondary calcination were the same as those of the primary calcination. The calcined powder was granulated by adding an appropriate amount of polyvinyl alcohol (PVA) binder and was pressed into a thin disc-shaped ceramic body with a pressure of 10 MPa. After burning off the binder at 600°C, the body was sintered at a high temperature of 1140°C for 4 h to obtain the desired ceramic blanks. Figure 1 shows the process flow diagram for KNN-xSBN preparation. The thickness of the polished sintered ceramic samples was reduced to 0.3 mm to test the optical properties, phase structure, and microscopic topography of the sample surface. In order to test its electrical properties, silver electrodes were plated on both sides of the samples.

The optical transmittance of the sample was tested in the range of 200–1100 nm using an ultraviolet–visible photometer, and the optical bandgap of the sample was calculated. The phase structure of the samples was analyzed by x-ray diffraction (XRD) technology (Bruker D8 Advance X, Germany), and the diffraction angle was 20°–80°. The microscopic topography of the sample surface was observed using a field emission scanning electron microscope (Quanta 450, USA), and the average grain size of the sample was calculated. The P–E hysteresis loops of the samples were tested by a ferroelectric test system at room temperature with a voltage of 80 kV. The energy storage density and efficiency were calculated with the hysteresis loop integration.

Results and Discussion

Figure 2 shows the XRD patterns of the ceramic samples when the KNN-SBN ceramics were dissolved with different content of the second component. The 20°–80° XRD patterns of KNN-SBN ceramics were tested at room temperature. In Fig. 2a, it can be seen that the ceramic has eight standard diffraction peaks of perovskite structure and no other impurity peaks, which indicates that the second
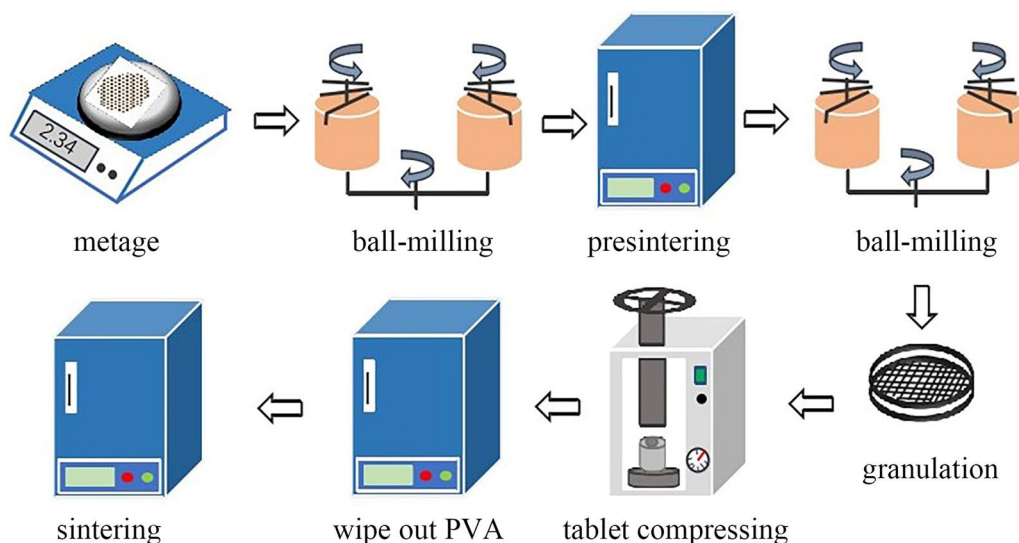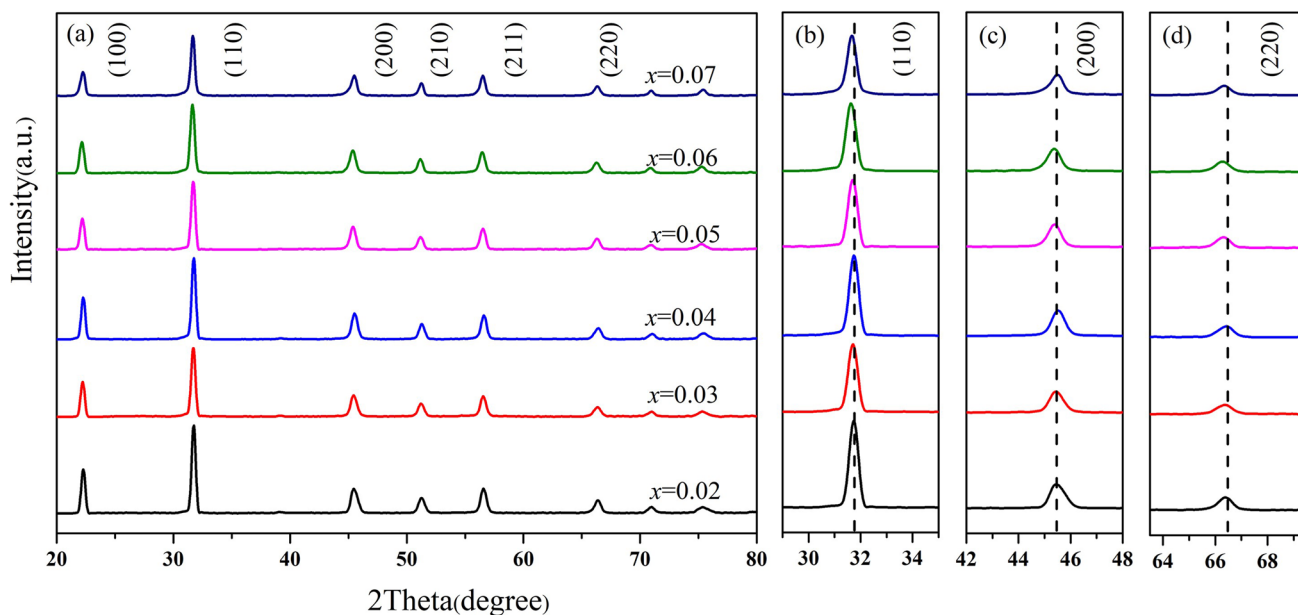
Fig. 1 Process flow diagram for KNN-xSBN preparation.

Fig. 2 (a) XRD pattern of KNN-xSBN ceramics; (b) magnified XRD pattern in the 2θ range at 29°–35°; (c) magnified XRD pattern in the 2θ range at 42°–48°; and (d) magnified XRD pattern in the 2θ range at 64°–69°.

component of SBN with different content is integrated into the KNN unit cell to form a uniform structure. The dominant diffraction peak (110) shifts to a lower angle as x content increases from 0.02 to 0.07, further implying the solid solution of SBN in host lattice the solid solution does not form a second phase. The (200) and (220) diffraction peaks reflect the phase structure of ceramic samples and they do not split, showing that the KNN-SBN ceramics preserve the pseudo-cubic phase's crystal structure. The solid solution does not form a second phase. The (200) diffraction peaks reflect the

phase structure of ceramic samples.[32] In order to better study the changes in the phase structure of ceramic samples with the increase in the second component solid solution content, the (200) diffraction peak is enlarged in Fig. 2b. It can be seen that the ceramic samples of all compositions have a unimodal structure. This shows that the solid solution of the second component SBN in KNN ceramics can effectively adjust its phase structure, so that all components of KNN-SBN ceramics are in a pseudo-cubic phase structure with light isotropy and good light transmission potential. With

the increase in the solid solution amount of the second component, the (200) diffraction peak gradually shifts to a large angle, which may be caused by the generation of oxygen vacancies and the shrinkage of the unit cell.[33-35] Since the valence state of the B-position $(Bi_{0.5}Nb_{0.5})^{4+}$ of the second component is different from the valence state of Nb^{5+} in the KNN-based unit cell, oxygen vacancies will appear when ion replacement occurs during the solid solution of the second component into the KNN unit cell to make up for the lack of valence. In order to study the changes in the crystal structure of KNN-SBN ceramics, the lattice parameters (a, b, c), the ratio of c/a, and the cell volume (V) were calculated, and the results are shown in Table I. It can be seen that when x is from 0.02 to 0.03, the unit cell gradually shrinks due to the generation of oxygen vacancies, and the XRD peak gradually shifts to the right at a large angle. From 0.03 to 0.05, the unit cell gradually expands due to oxygen vacancies to compensate for the lack of a valence state, and the peak position shifts to a low angle. From 0.06 to 0.07, the unit cell volume gradually shrinks due to the increase in oxygen vacancies, and the peak position shifts to the right. The pseudo-cubic phase with high symmetry can help incident light penetrate the ceramic sample better, and the fine grain size and good microstructure also have an important influence on the incident light passing through the ceramic.[36]

Figure 3 shows the microstructures of KNN-SBN ceramic samples with different solid solution content of the second component. As can be seen from the scanning electron microscope photo of KNN-SBN ceramic in Fig. 3, the grains of the ceramic samples of all composition points are uniformly distributed and have a relatively dense microstructure. It can be seen that the addition of the second component SBN significantly inhibits the grain growth, and the average grain size reaches the micrometer level. The average grain size of the ceramic samples gradually increases with the increase in the SBN solid solution content, which leads to a gradual decrease in its density. For some compositions where the SBN solid solution content is relatively large (such as $x = 0.06, 0.07$), some pores and defects can be clearly seen on the surface of the ceramic sample, and these defects or pores generate new scattering centers for incident light, which is not conducive to the transmission of incident light. The reason why the grain size gradually increases with the increase in the solid solution content of the second component may be due to the valence difference between Sr^{2+} occupying the A position of the second component and K^+ and Na^+ occupying the A position in the KNN unit cell.[37] When the solid solution content increases, a large number of vacancies are generated in the KNN unit cell, resulting in excessive grain growth during the sintering process. A large number of voids appeared on the surface of the ceramic sample at $x = 0.05$, which may be due to the fact that the surface of the ceramic

Table I The lattice parameters of KNN-xSBN ceramics

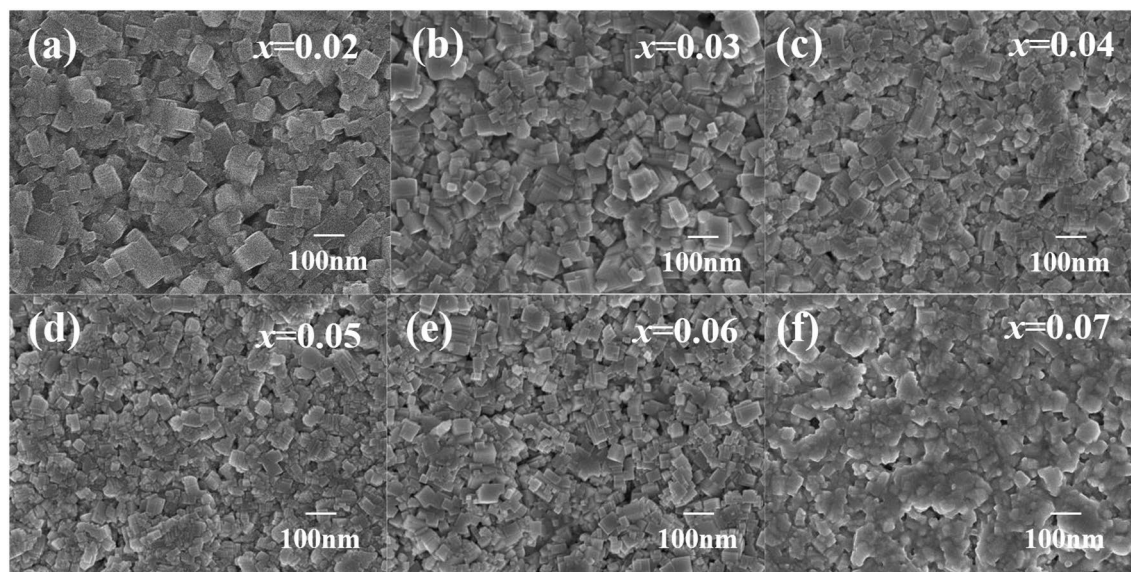| x	a (Å)	b (Å)	c (Å)	V (Å³)	c/a
0.02	3.9747	3.9700	3.9796	62.80	1.0012
0.03	3.9719	3.9690	3.9693	62.10	0.9993
0.04	3.9763	3.9831	3.9680	62.85	0.9979
0.05	3.9826	3.9858	3.9789	63.16	0.9991
0.06	3.9824	3.9861	3.9819	63.21	0.9999
0.07	3.9710	3.9860	3.9815	63.02	1.0037

Fig. 3 (a–f) Surface micromorphology and grain size distribution of KNN-xSBN ceramics ($x = 0.02, 0.03, 0.04, 0.05, 0.06, 0.07$).

sample was not completely covered with pre-fired powder before sintering, resulting in the volatilization of K$^+$ and Na$^+$ on the surface of the ceramic sample during the sintering process. In order to further study the effect of SBN content on ceramic grain size, we measured the grain size. Figure 4 shows the average grain size of KNN-xSBN. When $x = 0.02$, the largest grain diameter is 425.81 nm, the smallest is 40.07 nm, and the average grain size is 136.52 nm. The size of the grains varies greatly, and the grain distribution is uneven, so the transmittance of ceramics is low. When $x = 0.06$, large grains disappear, and the grains are evenly distributed. With a continued increase in SBN content, the average grain size of the ceramic increases slightly, and the grain distribution is uniform. The formula of ceramic density is as follows:

$$\rho = \frac{4m}{\pi d^2 h} \tag{1}$$

where m is the quality of the ceramic, h is the thickness, and d is the diameter. Figure 5 shows the effect of SBN doping on the density of the ceramic. It can be seen that when increasing amounts of SBN are added, the density of the ceramics becomes lower and lower, showing a clear decreasing trend. The introduction of SBN may cause inhomogeneous crystal growth, formation of pores or defects, and thus a decrease in the density of the ceramic.

Figure 6 shows the optical transmittance of KNN-SBN ceramic samples tested in the range of 200–1100 nm. Figure 6a shows the physical figure of the ceramic sample, and the letters at the bottom of the ceramic sheet can be clearly
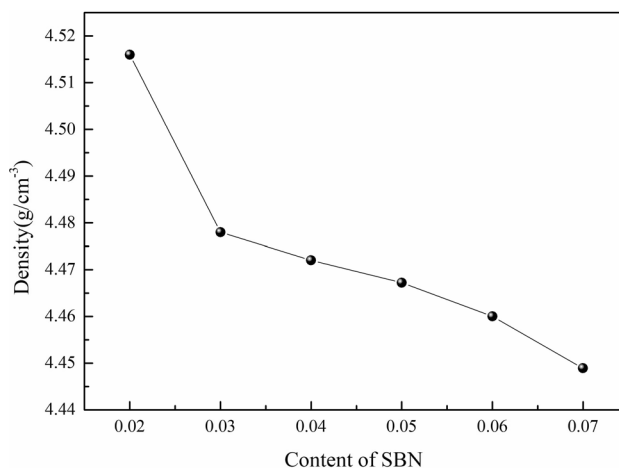
Fig. 5 The ceramic density of KNN-xSBN.

seen, which indicates that the KNN-SBN ceramic samples have a certain light transmittance in the visible light band. Figure 6b shows that the transmittance of the ceramic sample gradually decreases with the decrease in the wavelength of the incident light, and the transmittance of all samples is close to zero around 400 nm, which is caused by inter-band transitions.[38] It can be seen in Fig. 6c that all KNN-SBN ceramics have good transmittance, which is consistent with the phenomenon of the actual image of the ceramic samples in Fig. 6a. It can be seen that with the increase in the solid solution amount of the second component SBN, the transmittance of the ceramic sample increases first and then
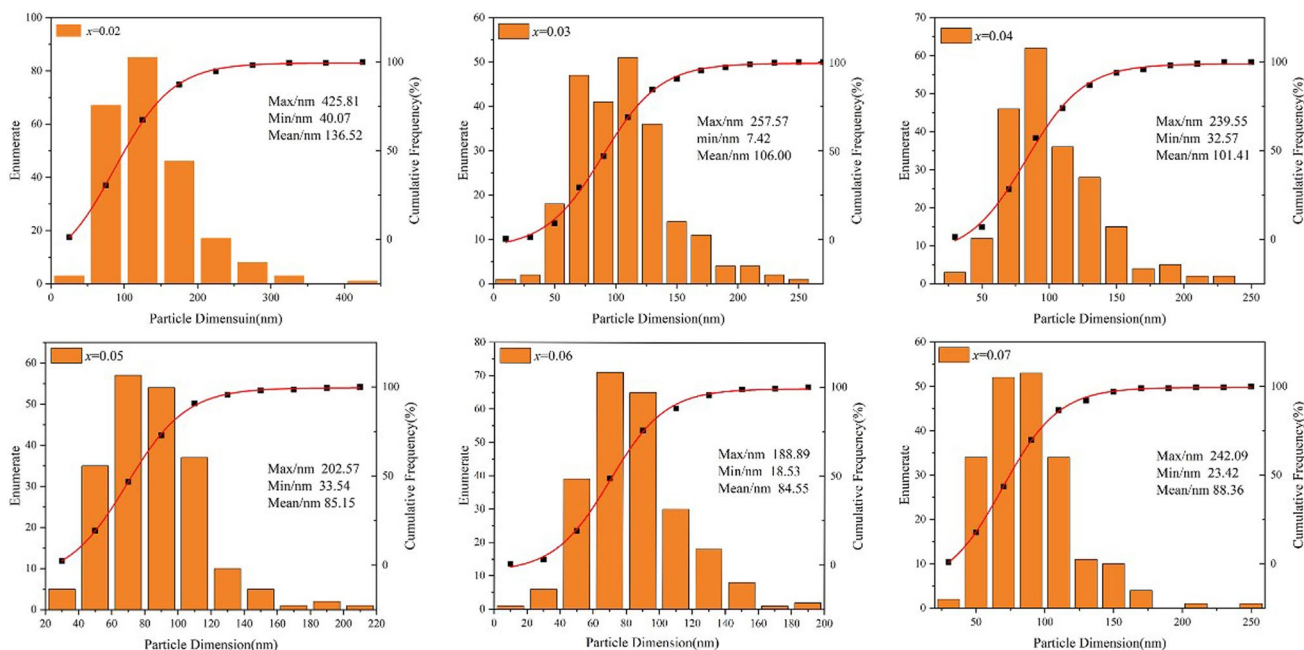
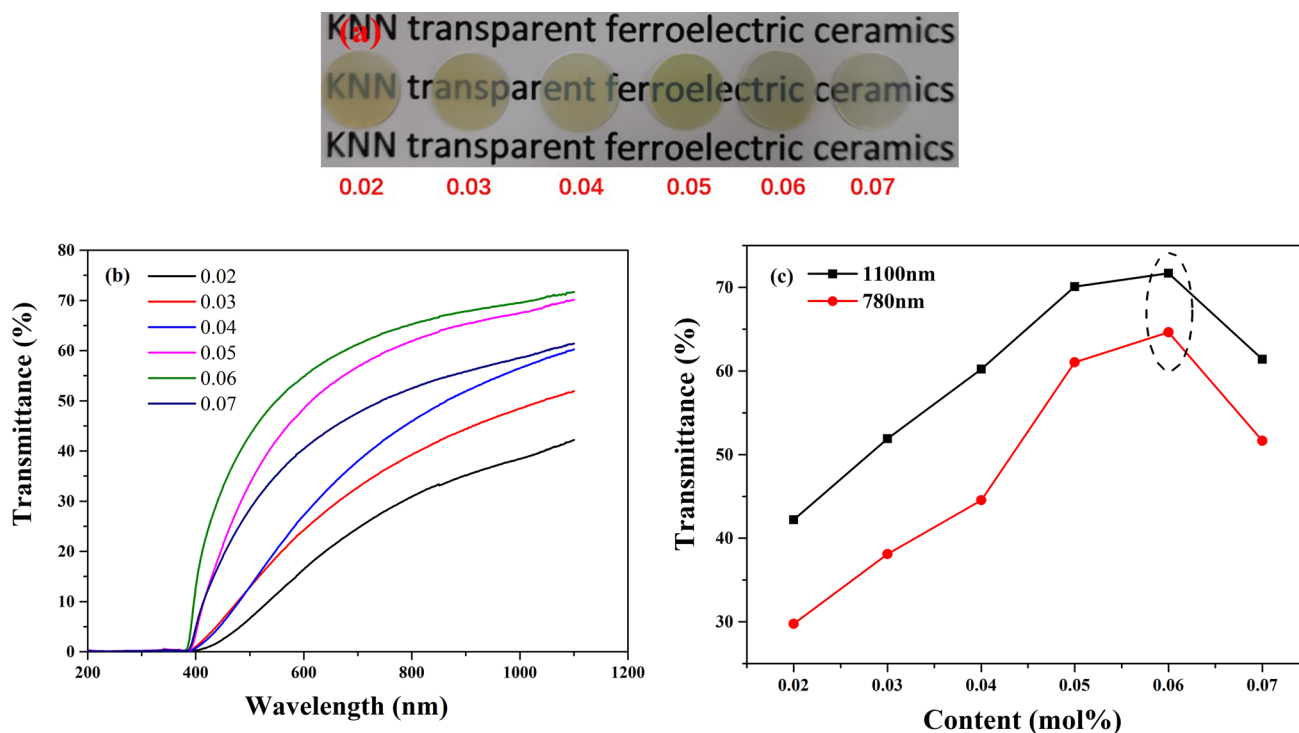**Fig. 4** The corresponding distribution of grain size of KNN-xSBN ceramics.

Fig. 6 (a) Photograph of the KNN-xSBN transparent ceramics. (b) and (c) The variation curves of transmittance (%) with wavelength (nm) in the range of 200–1100 nm and content (x), respectively.

decreases, and the transmittance is highest when $x = 0.06$. The transmittance in the near-infrared band (1100 nm) reaches a maximum of about 70%, and the transmittance in the visible light band (780 nm) reaches about 60%. Continuing to increase the solid solution content of the second component, the transmittance of the ceramic sample begins to decrease.

According to the absorption spectrum, the optical bandgap E_g can be calculated by using the Tauc equation.[39] For direct transition, the relationship between absorption coefficient α and E_g can be expressed as

$$(hv\alpha)^2 = A\left(hv - E_g\right) \tag{2}$$

where h is Planck's constant, v is the photon frequency, and A is a constant. The absorption coefficient can be calculated using the transmittance T, and the formula is as follows:

$$\alpha = \frac{1}{t}\ln\frac{1}{T} \tag{3}$$

where t is the thickness of the sample. According to the relationship between $(hv\alpha)^2$ and hv, E_g can be determined by drawing the linear equation and extrapolating the linear portion of the curve to zero. The transmittance of ceramics is closely related to the bandgap energy. Although a large bandgap energy is not conducive to the transition of

electrons between the valence band and the conduction band, it increases the energy of photon transport. Thus, the ceramics have high light transmittance.[40] It can be seen in Fig. 7 that the E_g value of ceramics is between 3.05 eV and 3.16 eV. With the increase in SBN doping content, the E_g value increases first and then decreases. The change in E_g value is consistent with the change in ceramic light transmittance. Figure 8 shows the calculated KNN-SBN energy band structure. It shows the simulated structure of KNN-SBN optimized in CASTEP, a computational module of the Materials Studio (MS) software, where the energy band structure of the optimized structure is calculated. It is evident that as x increases from 0.02 to 0.06, the value of E_g decreases. However, as x further increases from 0.06 to 0.07, the value of E_g increases. This calculation result is highly consistent with the experimental findings of the optical bandgap variation.

Raman spectroscopy is very sensitive to the lattice vibration of ceramic samples in the short-range order, and is another effective way to analyze the phase structure of ceramic samples. Figure 9 shows the Raman spectrum of KNN-SBN ceramic samples in the range of 100–1000 cm^{-1}. Three distinct vibration peaks can be seen in the figure. The V5 vibrational peak around the Raman shift of 200^{-1} represents the vibrational mode of the A-position cation in the KNN unit cell. The V5 vibrational peak at the Raman shift of 600^{-1} mainly reflects the symmetric stretching mode of
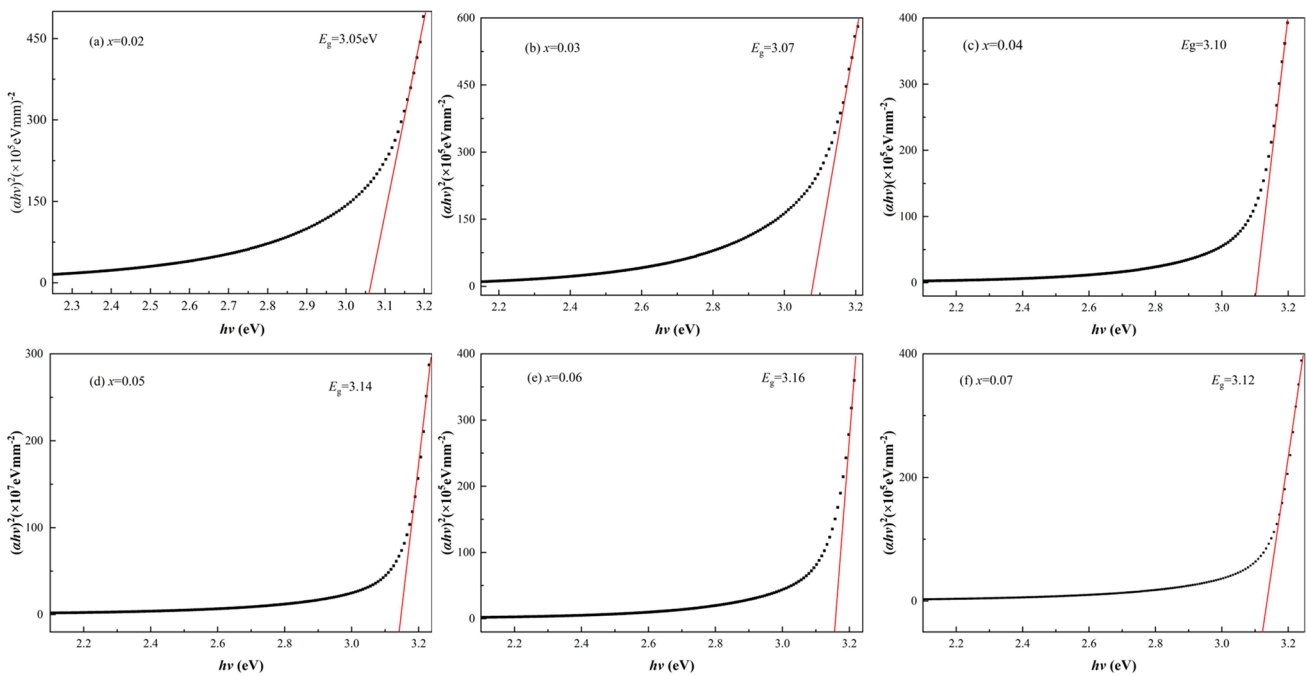
Fig. 7 (a–f) Optical bandgap diagrams of KNN-xSBN ceramic ($x=0.02, 0.03, 0.04, 0.05, 0.06, 0.07$).
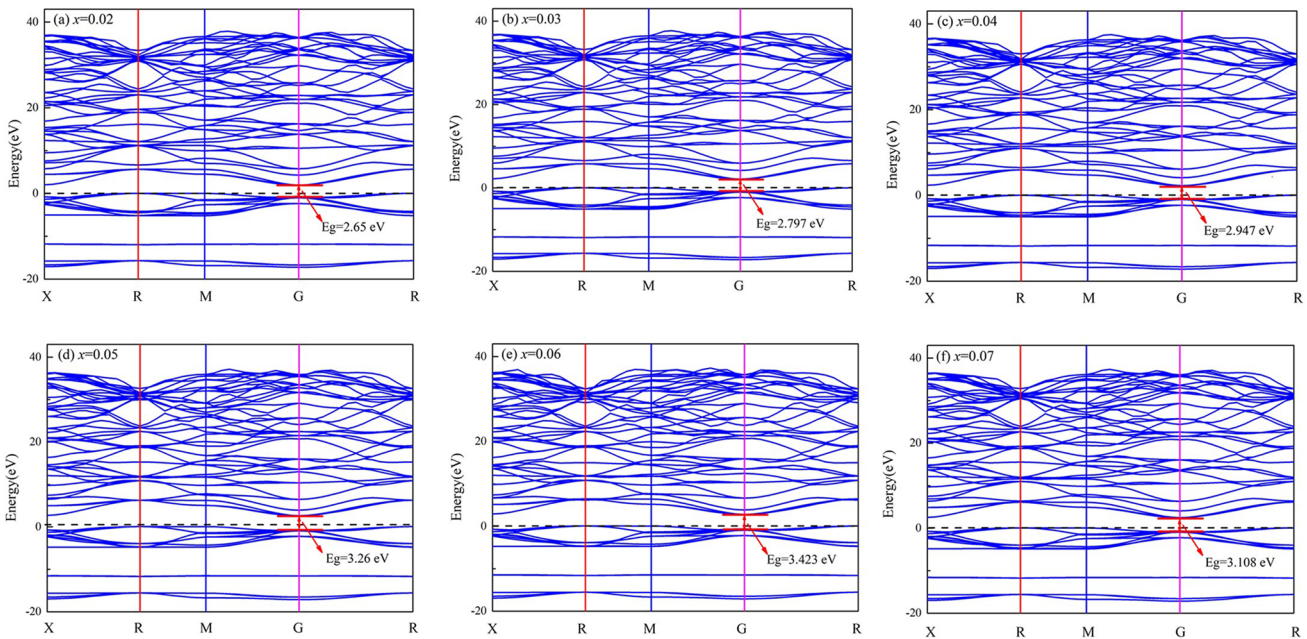

Fig. 8 (a–f) Theoretical values of optical bandgap diagrams of KNN-xSBN ceramic ($x=0.02, 0.03, 0.04, 0.05, 0.06, 0.07$).

the NbO$_6$ octahedron. The vibration peaks of the ceramic samples with different composition in the figure have the vibration mode of the ABO$_3$ type of perovskite structure. With the increase in the solid solution content of the second component SBN, the A-position cation vibrational peaks and the NbO$_6$ octahedral vibrational peaks gradually changed from sharp to gentle and shifted to low angles. This shows that the degree of distortion of the NbO$_6$ octahedron is reduced, and the symmetry of the phase structure of the ceramic sample is gradually enhanced. The pseudo-cubic phase is a phase structure in which the tetragonal phase and the cubic phase coexist. The enhanced phase structure
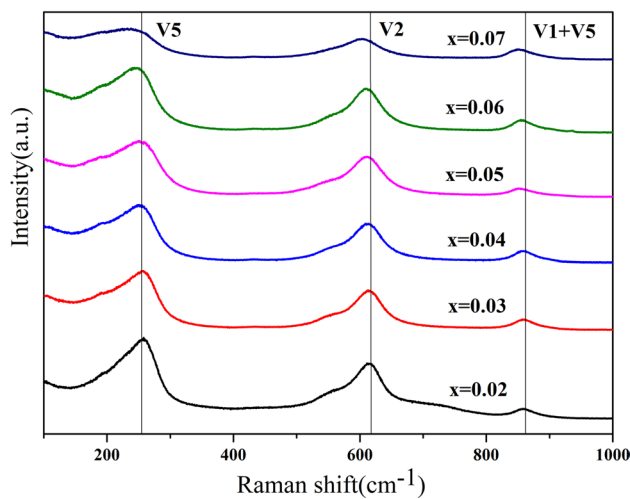
Fig. 9 Raman spectrum of KNN-xSBN ceramics.

symmetry of the ceramic sample indicates that the phase structure gradually transforms to a cubic phase, which is also consistent with the XRD analysis results in the previous section.

Figure 10 shows the P–E hysteresis loops of KNN-SBN ceramic samples at room temperature, and the test voltage range is 30–130 kV; P_{max} is the saturation polarization, P_r is the remanent polarization, and E_c is the coercive field. In Fig. 10a, it can be seen that the P_{max} of the KNN-SBN ceramic sample reaches a maximum of 30 μC/cm^2, and the P_r values of all the ceramic samples are below 6 μC/cm^2. This is due to the fact that the Bi^{3+} doping in the second component enables the ceramic sample to have large P_{max} while maintaining small P_r. With the increase in the solid solution content of the second component, the slender ferroelectric properties of the P–E hysteresis loop of the ceramic samples gradually decreased, and the P_{max} gradually decreased from 30 μC/cm^2 to 10.1 μC/cm^2.

P_r changes from 6.587 μC/cm^2 to 1.532 μC/cm^2, and E_c from 17.42 kV/cm to 12.21 kV/cm. The ferroelectric properties of the KNN-SBN ceramic samples weakened with the addition of the second component, which was due to the gradual transformation of the phase structure from tetragonal to cubic.[41] The ferroelectric properties of the material are more dependent on the asymmetric ferroelectric tetragonal phase structure, and the paraelectric cubic phase with symmetry will weaken the ferroelectric properties of the material. Figure 11 shows the temperature-dependent dielectric constant (ε_r) and loss (tanδ) of the KNN-xSBT ceramics at test frequencies of 10 kHz, 50 kHz, 100 kHz, and 200 kHz. With the increase in the second component SBN, the double peaks merge into a broad peak, which is considered as evidence for the transition from a ferroelectric to relaxor ferroelectric.[42] The changes in the ferroelectric properties of the ceramic samples are also consistent with the XRD analysis results in the previous section.

The recoverable energy storage density W_{rec} and energy storage efficiency η of the KNN-SBN ceramic sample were calculated according to the P–E hysteresis loop.[43] The energy storage density W of ceramics can be estimated using the following formula[44]:

$$W = \int_0^{P_{max}} E\,dP \tag{4}$$

where E is the electric field, and P is the polarization. The recyclable energy storage density W_{rec} can be estimated by the following:

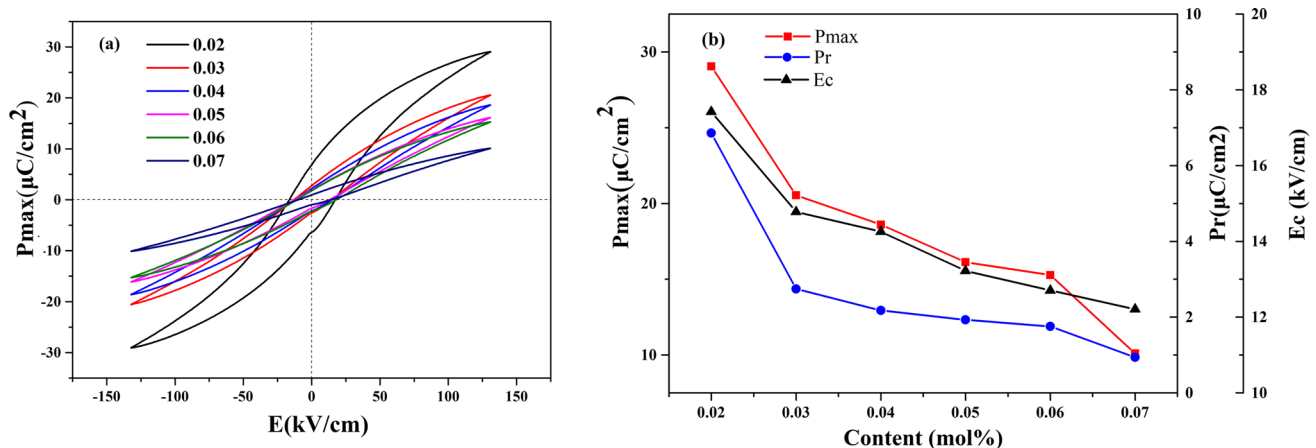$$W_{rec} = \int_{P_r}^{P_{max}} E\,dP \tag{5}$$

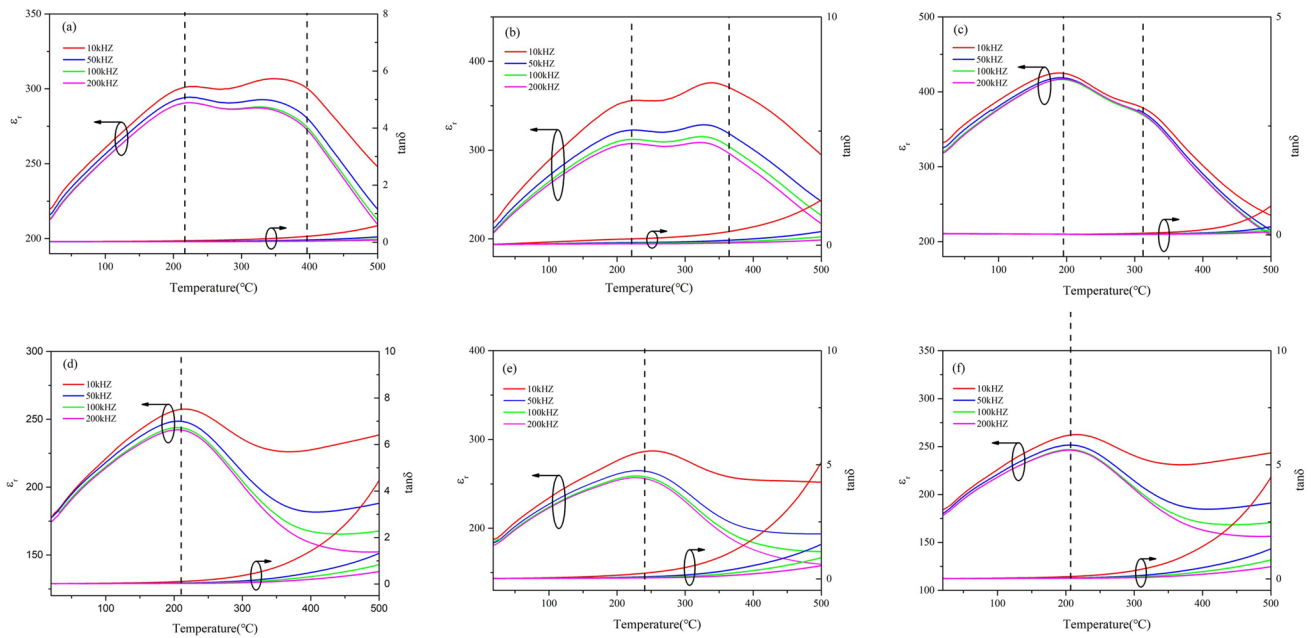**Fig. 10** KNN-xSBN ceramics under 80 kV/cm electric field: (a) PE hysteresis loops and (b) variation trends of P_m and P_r with content (x).

Fig. 11 Temperature dependence of dielectric constant (ε_r) of KNN-xSBN ceramics at 10 kHz, 50 kHz, 100 kHz, and 200 kHz.
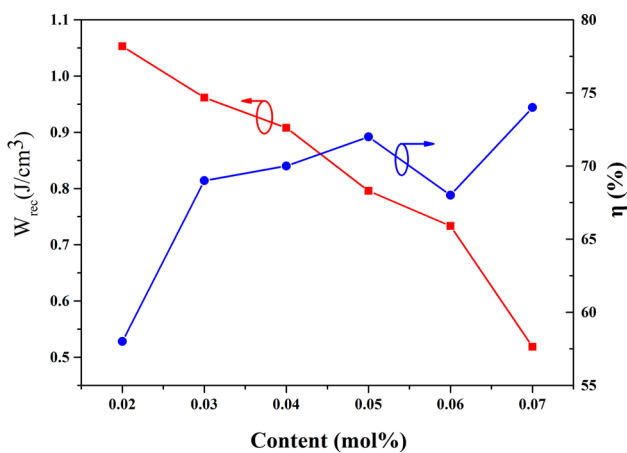

Fig. 12 Energy storage properties of KNN-xSBN ceramics.

Energy storage efficiency η is an important parameter to measure the energy storage performance of the material, and its calculation formula is

$$\eta = \frac{W_{rec}}{W} = \frac{W_{rec}}{W_{rec} + W_{loss}} \times 100\% \tag{6}$$

In Fig. 12, it can be seen that all the KNN-SBN ceramics have certain energy storage performance. When $x = 0.02$, the W_{rec} of the ceramic sample reaches a maximum of 1.05 J/cm^3. After that, with the increase in the

solid solution content of the second component SBN, W_{rec} gradually decreased. When $x = 0.06$, W_{rec} drops to 0.75 J/cm^3. When $x = 0.07$, W_{rec} is 0.52 J/cm^3. The energy storage efficiency η showed a gradual upward trend with the increase in the value of the second component x. When $x = 0.02$, the energy storage efficiency of ceramics was 58%, and when $x = 0.06$ and 0.07, the energy storage efficiency of ceramic samples increased to 68% and 74%, respectively.

Conclusion

The results show that a ferroelectric ceramic material with good light transmission properties was successfully prepared by solid solution of the second component Sr(Bi$_{0.5}$Nb$_{0.5}$)O$_3$ in (K$_{0.5}$Na$_{0.5}$)NbO$_3$ ceramics. According to the XRD results, the addition of the second component SBN successfully regulated the phase structure of KNN ceramics, making it transform from tetragonal phase structure to cubic phase structure, resulting in KNN-SBN ceramics in a pseudo-cubic phase structure with optical isotropy. The transmittance of KNN-SBN ceramics reaches the highest when the second component solid solution content $x = 0.06$. The highest transmittance in the near-infrared band reaches 71.68%, and the transmittance in the visible light band reaches 64.64%. The transmittance increases first and then decreases with the increase in the solid solution content of the second component SBN. When $x = 0.06$, the P_{max} of the ceramic sample is 15.27

$\mu C/cm^2$, $P_r = 1.752$ $\mu C/cm^2$, and $E_c = 12.7$ kV/cm^2. The energy storage efficiency η of the ceramic samples reaches the highest value of 74% at $x = 0.07$. When $x = 0.06$, $W_{rec} = 0.75$ J/cm^3, and η = 68%. The composition with the highest light transmittance also has good electrical properties and is an excellent multifunctional material.

Conflict of interest The authors declare no competing financial interests.

References

1. J. Zhan, L.Q. An, M. Liu, S. Shimai, and S.W. Wang, Sintering of Yb^{3+}: Y$_2$O$_3$ transparent ceramics in hydrogen atmosphere. *J. Eur. Ceram. Soc.* 29, 305–309 (2009).

2. Y. He, Y.X. Cai, L. Zhang, K.G. Liu, G. Liu, B.X. Xiang, J.P. Zhai, L.B. Kong, T.S. Zhang, and Y. Liu, Rapid fabrication of extremely thin Nano-Al$_2$O$_3$ transparent ceramic wafers through nonaqueous tape casting. *Ceram. Int.* 47, 30677–30684 (2021).

3. S. Chen and Y. Wu, New opportunities for transparent ceramics. *J. Am. Ceram. Soc. Bull.* 92, 32–37 (2013).

4. H.T. Wu, G.B. Hu, S.Y. Shi, X. Liu, H. Wang, J.W. Xu, L. Yang, W. Qiu, and S.J. Zhou, Effect of Ho addition on the optical and electrical properties of 0.98KNN-0.02SYT ceramics. *J. Electron. Mater.* 51, 831–837 (2022).

5. G.R. Li, W. Ruan, J.T. Zeng, H.R. Zeng, L.Y. Zheng, L.S. Kamzina, Y. Kopylov, and V. Kravchenko, The effect of domain structures on the transparency of PMN-PT transparent ceramics. *Opt. Mater.* 35, 722–726 (2013).

6. C.Y. Li, M.W. Yao, W.B. Gao, and X. Yao, High breakdown strength and energy density in antiferroelectric PLZST ceramics with Al$_2$O$_3$ buffer. *Ceram. Int.* 46, 722–730 (2020).

7. Y.B. Sun, H. Wang, G.B. Liu, H. Xie, C.R. Zhou, G.H. Chen, C.L. Yuan, and J.W. Xu, High energy storage efficiency and high electrostrictive coefficients in BNT-BS-xBT ferroelectric ceramics. *J. Mater. Sci. Mater. Electron.* 31, 5546–5553 (2020).

8. X. Zeng, X.Y. He, W.X. Cheng, P.S. Qiu, and B. Xia, Effect of Dy substitution on ferroelectric, optical and electrooptic properties of transparent Pb$_{0.90}$La$_{0.10}$ (Zr$_{0.65}$Ti$_{0.35}$) O$_3$. *Ceram. Int.* 40, 6197–6202 (2014).

9. H. Ji, W. Ren, L. Wang, P. Shi, X. Chen, X. Wu, and X. Yao, Effect of Dy substitution on ferroelectric, optical and electrooptic properties of transparent Pb$_{0.90}$La$_{0.10}$ (Zr$_{0.65}$Ti$_{0.35}$) O$_3$. *J. Am. Ceram. Soc.* 94, 3425–3430 (2011).

10. Y. Cao, K. Zhu, H. Zheng, J. Qiu, and H. Gu, Synthesis of potassium sodium niobate powders using an EDTA/citrate complexing Sol–Gel method. *Particuology* 10, 777–782 (2012).

11. Y. Hou, C. Wang, J. Zhao, H. Ge, M. Zhu, and H. Yan, The fine-grained KNN-LN ceramics densified from nanoparticles obtained by an economical sol–gel route. *Mater. Chem. Phys.* 134, 518–522 (2012).

12. L. Bai, K. Zhu, J. Qiu, H. Ji, and L. Su, Phase evolution of (K, Na) NbO$_3$ powder prepared by high temperature mixing under hydrothermal conditions. *Particuology* 8, 477–481 (2010).

13. G. Stavber, B. Malic, and M. Kosec, A road to environmentally friendly materials chemistry: low-temperature synthesis of nano-sized K$_{0.5}$Na$_{0.5}$NbO$_3$ powders through peroxide intermediates in water. *Green Chem.* 13, 1303–1310 (2011).

14. M.R. Kannan, A. Logeswari, M. William Carry, and T. Vijaya-kumar, Synthesis and investigation of (1−x)K$_{0.5}$Na$_{0.5}$NbO$_3$−(x) CaSnO$_3$ lead free perovskite ceramics of high dielectric and piezoelectric properties for transducer applications. *J. Mater. Sci. Mater. Electron.* 33, 9224–9234 (2022).

15. L. Gao, W.C. Zhou, F. Luo, D.M. Zhu, and J. Wang, Dielectric and microwave absorption properties of KNN/Al$_2$O$_3$ composite ceramics. *Ceram. Int.* 43, 12731–12735 (2017).

16. X.Z. Wang, Y. Huan, Z.X. Wang, X.J. Lin, S.F. Huang, T. Wei, L.T. Li, and X.H. Wang, Electrical conduction and dielectric relaxation mechanisms in the KNN-based ceramics. *J. Appl. Phys.* 126, 104101 (2019).

17. Z.C. Sun, B.J. Xu, F. Jin, G.X. Zhou, and L. Lin, Machine learning approach for on-demand rapid constructing metasurface. *IEEE J. Sel. Top. Quantum Electron.* 28, 1–9 (2022).

18. J. Du, J.F. Wang, G.Z. Zang, and X.J. Yi, Ca$_{0.5}$Sr$_{0.5}$TiO$_3$-modified KNN-based lead-free piezoceramics with a wide temperature usage span. *J. Wuhan Univ. Technol. Mater. Sci. Ed.* 28, 067701 (2011).

19. H.N. Liu, J.T. Wang, H. Wang, J.W. Xu, C.R. Zhou, and W. Qiu, Er^{3+} and Sr(Bi$_{0.5}$Nb$_{0.5}$)O$_3$-modified (K$_{0.5}$Na$_{0.5}$)NbO$_3$: a new transparent fluorescent ferroelectric ceramic with high light transmittance and good luminescence performance. *Ceram. Int.* 48, 4230–4237 (2022).

20. D. Yang, C. Ma, Z. Yang, L. Wei, X. Chao, Z. Yang, and J. Yang, Optical and electrical properties of pressureless sintered transparent (K$_{0.37}$Na$_{0.63}$)NbO$_3$-based ceramics. *Ceram. Int.* 42, 4648–4657 (2016).

21. M. Kosec, V. Bobnar, M. Hrovat, J. Bernard, B. Malic, and J. Holc, New lead-free relaxors based on the K$_{0.5}$Na$_{0.5}$Nb$_{0.30}$-SrTi$_{0.3}$ solid solution. *J. Mater. Res.* 19, 1849–1854 (2004).

22. F. Li and K.W. Kwok, Fabrication of transparent electro-optic (K$_{0.5}$Na$_{0.5}$)1−xLi$_x$Nb$_{1−x}$ BixO$_3$ lead-free ceramics. *J. Eur. Ceram. Soc.* 33, 123–139 (2013).

23. Q.Z. Chai, X.M. Zhao, P.F. Liang, D. Wu, X.L. Chao, and Z.P. Yang, Excellent near-infrared transparency realized in low-symmetry orthorhombic (K, Na)NbO$_3$-based submicron ceramics. *Scr. Mater.* 154, 64–67 (2018).

24. F.G. Mohammadi, and M.S. Abadeh, A new metaheuristic feature subset selection approach for image steganalysis. *J. Intell. Fuzzy Syst.* 27, 1445–1455 (2014).

25. K.W. Kwok, F. Li, and D. Lin, A novel lead-free transparent ceramic with high electro-optic coefficient. *Funct. Mater. Lett.* 04, 237–240 (2011).

26. H. Du, W. Zhou, D. Zhu, L. Fa, S. Qu, and Y. Li, *J. Am. Ceram. Soc.* 91, 2903–2909 (2008).

27. R.Z. Zuo, X.S. Fang, and C. Ye, Phase structures and electrical properties of new lead-free (Na$_{0.5}$K$_{0.5}$)NbO$_3$-(Bi$_{0.5}$Na$_{0.5}$)TiO$_3$ ceramics. *Appl. Phys. Lett.* 90, 092904 (2007).

28. D. Damjanovic, N. Klein, J. Li, and V. Porokhonskyy, What can be expected from lead-free piezoelertic materials? *Funct. Mater. Lett.* 3, 5–13 (2010).

29. H.T. Wu, S.Y. Shi, X. Liu, H. Wang, J.W. Xu, L. Yang, W. Qiu, and S.J. Zhou, The Ba(Bi$_{0.5}$Ta$_{0.5}$)O$_3$ modified (K$_{0.5}$Na$_{0.5}$)NbO$_3$ lead-freetransparent ferroelectric ceramics with high transmittance and excellent energy storage performance. *J. Mater. Sci. Mater. Electron.* 33, 16045–16055 (2022).

30. G.B. Hu, H.N. Liu, J.T. Wang, Y.B. Sun, H. Wang, J.W. Xu, and L. Yang, Regulating the structural, regulating the structural, transmittance, ferroelectric, and energy storage properties of K$_{0.5}$Na$_{0.5}$NbO$_3$ ceramics using Sr(Yb$_{0.5}$Nb$_{0.5}$)O$_3$. *J. Electron. Mater.* 50, 968–977 (2021).

31. G.B. Hu, J.T. Wang, X. Liu, H.N. Liu, H. Wang, J.W. Xu, L. Yang, C.R. Zhou, and W. Qiu, Structural, transmittance, ferroelectric, energy storage, and electrical properties of $K_{0.5}Na_{0.5}NbO_3$ ceramics regulated by $Sr(Yb_{0.5}Ta_{0.5})O_3$. *J. Mater. Sci. Mater. Electron.* 32, 22300–22308 (2021).

32. J.F. Lin, P. Wang, H.J. Wang, Y.J. Shi, K. Zhu, F. Yan, G.H. Li, H.H. Ye, J.W. Zhai, and X. Wu, Significantly photo-thermochromic knn-based "smart window" for sustainable optical data storage and anti-counterfeiting. *Adv. Opt. Mater.* 9, 2100580 (2021).

33. X.L. Chao, X.D. Ren, X.S. Zhang, Z.H. Peng, J.J. Wang, P.F. Liang, D. Wu, and Z.P. Yang, Excellent optical transparency of potassium-sodium niobate-based lead-free relaxor ceramics induced by fine grains. *J. Eur. Ceram. Soc.* 39, 3684–3692 (2019).

34. T. Huang, D.Q. Xiao, W.F. Liang, J.G. Wu, Z. Wang, and J.G. Zhu, Sintering behavior of KNN-BNKT lead-free piezoelectric ceramics. *Ferroelectrics* 458, 37–42 (2014).

35. J.H. Xing, F. Shang, L. Li, and G.H. Chen, Structure, up-conversion luminescence and optical temperature sensitive properties of glass ceramics containing $Ca_5(PO_4)_3F$ with double luminescence centers. *Ceram. Int.* 48, 1098–1106 (2022).

36. M. Zhang, H.B. Yang, D. Li, and Y. Lin, *J. Alloys Compd.* 829, 154565 (2020).

37. X. Vendrell, J.E. García, E. Cerdeiras, D.A. Ochoa, F. Rubio-Marcos, J.F. Fernández, and L. Mestres, Effect of lanthanide doping on structural, microstructural and functional properties of $K_{0.5}Na_{0.5}NbO_3$ lead-free piezoceramics. *Ceram. Int.* 42, 17530–17538 (2016).

38. D. Yang, Z. Yang, X. Zhang, L. Wei, and X. Chao, High transmittance in lead-free lanthanum modified potassium-sodium niobate ceramics. *J. Alloys Compd.* 716, 1249–1258 (2019).

39. X. Wu, J.F. Lin, P.F. Chen, C.W. Liu, M. Lin, C. Lin, L.H. Luo, and X.H. Zheng, Ho^{3+}-doped (K, Na)NbO_3-based multifunctional transparent ceramics with superior optical temperature sensing performance. *J. Am. Ceram. Soc.* 102, 1249–1258 (2019).

40. Z.M. Geng, K. Li, X. Li, and D.L. Shi, Fabrication and photoluminescence of Eu-doped KNN-based transparent ceramics. *J. Mater. Sci.* 52, 2285–2295 (2016).

41. A. Chitra, R. Khandelwal, R.L. Guupta, and K.C. Singh, Impact of crystal structure and microstructure on electrical properties of Ho doped lead-free BCST piezoceramics. *Ceram. Int.* 45, 10371–10379 (2019).

42. J. Zhang, J.W. Xu, L. Yang, Z.J. Cao, C.L. Yuan, C.R. Zhou, H. Wang, and G.H. Rao, Controlling light-induced dielectric response of Sr/Ni-modifed ($K_{0.5}Na_{0.5}$)NbO_3 ceramics by narrow bandgap method. *Mater. Sci. Semicond. Process.* 143, 106521 (2022).

43. J.L. Li, F. Li, Z. Xu, and S.J. Zhang, Multilayer lead-free ceramic capacitors with ultrahigh energy density and efficiency. *Adv. Mater.* 30, 1802155 (2018).

44. X. Hao, A review on the dielectric materials for high energy-storage application. *J. Adv. Dielectr.* 3, 1330001 (2013).